ELSEVIER

PII: S0032-3861(96)00999-8

Polymer Vol. 38 No. 16, pp. 4151–4164, 1997

0032-3861/97/$17.00 + 0.00

Macromolecular dynamics in extensional flows: 1. Birefringence and viscometry

S. P. Carrington, J.P. Tatham and J. A. Odell*
H.H. Wills Physics Laboratory, University of Bristol, Bristol BS8 1TL, UK

and A. E. Sáez
Department of Chemical Engineering, North Carolina State University, Raleigh, NC 27695-7905, USA
(Received 26 March 1996; revised 5 September 1996)

The opposed jets apparatus is used to investigate the dynamics of the coil-stretch transition of polymer solutions in an idealized stagnation point extensional flow-field. A linear CCD detector allows optical retardation profiles to be recorded as the strain rate is varied. A numerical transformation enables *true* birefringence profiles to be produced, which enable the assessment of localized molecular orientation and stretching around the stagnation point. High molecular weight, closely monodisperse aPS and PEO are studied in θ and good solvents. Flow modification effects are apparent to extremely low concentration ($\approx c^*/100$). Under θ conditions, the width of the transition is consistent with the residual polydispersity. Simultaneous measurements of flow resistance enable the determination of the effective extensional viscosity. The increase in extensional viscosity due to molecular stretching is found to be of the order of the number of equivalent flexible units in the chain, after correction is made for the area of high molecular extension. © 1997 Elsevier Science Ltd.

(Keywords: birefringence; viscometry; extensional flow)

INTRODUCTION

It has been long empirically established that solutions of parts per million of high molecular weight polymers can exhibit remarkable non-Newtonian behaviour. The most striking examples being the observation of turbulent drag reduction[1] and dramatic flow thickening beyond a critical flow-rate in porous media flows[2]. Such phenomena have tremendous commercial importance and have been attributed to, perhaps the most fundamental physical property of high polymers, that of extensibility. In stretching flows especially, a transition from an ambient coil state to a stretched out conformation might be expected to dramatically modify flow behaviour.

Theory and modelling of stretching macromolecules

Early theoretical works by James and Guth[3], and Flory[4] investigated the forces required to produce extension of individual chains. In 1961, Peterlin asserted that modelling of non-Newtonian properties required the introduction of a finite extensibility[5]. In a landmark paper in 1974, de Gennes predicted that the coil-stretch phenomenon in dilute solutions in stretching flow-fields could be critical, with a sudden transition from a coil to a close to fully extended state as the strain-rate is increased[6]. This he envisaged to be due to an increase in frictional interaction of the moving solvent with the coil as it begins to extend and become more free-draining—resulting in a run-away process. Hysteresis is predicted in the coil–stretch–coil cycle. Similar ideas were advanced in the same year by Hinch[7]. An enormous increase in extensional viscosity would be anticipated for the stretched out molecules.

In 1989, Brestkin used a non-linear dumb-bell model with varying friction coefficient on extension[8]. This method incorporated a system of spherical co-ordinates to avoid the Peterlin approximation used by de Gennes. The outcome was an S-shaped transition (i.e. showing hysteresis) critical in velocity gradient.

Magda *et al.* used a computational scheme for the distribution function of a bead-spring model with conformation dependent hydrodynamic interaction[9]. Their model also predicts a coil-stretch transition in steady extensional flow, with hysteresis in the value of extensional viscosity. This is in agreement with the dumb-bell models of de Gennes[6] and Hinch[7].

In 1990, Wiest *et al.* modelled polymer molecules as bead-spring chains with finitely extensible non-linear elastic springs, using the Peterlin approximation[10]. At a constant high strain rate, they observed a gradual transition from the coiled equilibrium chain to the stretched state, via locally deformed states. S-shaped curves were not observed, and these were attributed to a non-physical anomaly which arises as a consequence of the use of the Peterlin approximation for a dumb-bell[11]. The inclusion of hydrodynamic interaction did not qualitatively change the molecular response.

Liu used a stochastic approach as a basis for a Brownian dynamics simulation for a freely jointed bead-rod chain, with constant hydrodynamic interaction[12]. Liu found no evidence of an S-shaped (hysteresis) curve for the mean square end-to-end distance ($\langle r^2 \rangle$) as a function of elongation rate, but by neglecting the

* To whom correspondence should be addressed

changing friction coefficient on extension, this would not be totally unexpected. This work also attempted to calculate the extensional viscosity as the chain is stretched out. The models predicted that the viscosity would increase roughly linearly with N, the number of flexible links.

Darinskii *et al.* simulated the motion of a dumb-bell with conformation dependent friction coefficient, using the Brownian dynamics technique[13]. In contrast to Wiest *et al.*[10] they observed the S-shaped (hysteresis) curve for the extension ratio of the dumb-bell as a function of the velocity gradient (in agreement with de Gennes), when simulation times were comparable with the transition times.

Rallison and Hinch modelled the extensional viscosity for a FENE dumb-bell with and without a conformation dependant friction[14]. Without conformational friction dependence they again predicted extensional viscosity to scale with N, including the conformational dependence they predicted that the viscosity would scale with N^3. Only in the latter case was a hysteresis predicted in the stretching behaviour.

Hinch has reported computer simulations of chain uncoiling via 'kinks dynamics'[15]. Such a process could provide high birefringence levels at relatively low molecular strains. However, these flow simulations were clearly carried out in inappropriate regimes, and involve timescales for which local segmental orientation is likely.

There is clearly still no general consensus as to the criticality and hysteresis of the coil–stretch transition. Neither has a single picture of the mode or the final extension of stretching emerged. Furthermore, there is no universal agreement about the anticipated increase in the extensional viscosity.

Experimental observations

For a polymer molecule to achieve high chain extension in a stretching flow-field, there must be sufficient strain-rate maintained over a long enough time for a given fluid element to attain the required strain. If the molecule slips with respect to the fluid during the uncoiling process (i.e. non-affine molecular deformation), then the appropriate fluid strain would need to be greater than the strain for full molecular extension. By using a flow-field which incorporates a stagnation point, some fluid elements remain trapped within the flow-field over a long period of time. Such fluid elements are subject to the very high strains necessary for flexible coils to extend.

Flows which are purely extensional can be realized by uniaxial extension and pure shear. The former can be approximated by the opposed jets apparatus[16,17], where two symmetric jets, facing each other with a small separation, are immersed in a solution. Sucking the solution into both jets creates a strong uniaxial extensional flow field with cylindrical symmetry about the axis of the jet apertures. Velocities at the jet entrance can be very high, whilst the fluid is forced to accelerate from the stagnation point at the centre of the symmetry axis. A variation on this geometry is the cross-slot device where the jets are replaced by slots to give an approximation to planar extension or pure shear. Other works have utilized the G.I. Taylor 4-roll mill, which creates close to pure shear, but with relatively high Reynolds number[18].

Experimentally, the coil–stretch transition has been followed by measuring the birefringent intensity against strain rate in a well defined extensional flow field. Early work in the Bristol laboratory was carried out by Keller and co-workers[16,17,19]. Studies have also been made elsewhere, notably by Fuller, Leal and co-workers[20–22] and by Brestkin and co-workers[23].

The general observation is that, beyond a set value of strain-rate, an extremely localized birefringent strand is observed around the stagnation point. The strain-rate required in order to stretch the molecules is of the order of the reciprocal of their longest relaxation time. The localization arises from the large strains required to fully stretch high molecular weight polymers. These are only realized along streamlines that pass very close to the stagnation point.

These results have been interpreted as being largely consistent with the de Gennes hypothesis, reporting an essentially critical onset of stretching, and usually, saturated levels of birefringence corresponding to the theoretical maximum for the polymers concerned. The broadening of the transition has been found to be consistent with the residual polydispersity in the polymer sample[17,24,25].

Isolated macromolecules have been found to undergo close central scission around a stagnation point. This process has been successfully explained by a Thermally Activated Barrier to Scission (TABS) model[26]. This model assumes the molecules to be extended and calculates the combined effect of the accumulating molecular stress and temperature. The TABS theory can predict the frequency of scission as a function of position along the chain thereby yielding the molecular weight distribution of the fracture products, accounting qualitatively for the degradation of a number of synthetic polymers[27,28]. The theory can be tested by the use of perfectly monodisperse DNA solutions, and the fracture products well characterized by the use of Pulsed Gel Electrophoresis (PGE). The DNA was progressively overstretched in an extensional flow-field until fracture occurred. PGE reveals precise halving and quartering of the molecules, and furthermore, TABS theory fully explains the distribution of scission products[29].

Recently Larson *et al.* reported novel experiments directly viewing the conformation of ultra high molecular weight DNA in applied flow-fields[30]. DNA is usually considered as a work-like molecule, but these extremely long molecules can be taken as large models of the flexible random coil. The molecule was subjected to a uniform flow, with one end held in 'optical tweezers'. Chain extension was seen to approach 90% completion.

Nguyen *et al.* have recently claimed that progressive segmental orientation causes a broadening of the transition and that the critical strain rate has no physical meaning[31]. A comparison of extensional flow with g.p.c. characterization has been put forward as evidence supporting this view. Nguyen *et al.* further claim that the saturation birefringence (B_0) is five times lower than theoretical expectations for fully stretched chains. This has been interpreted as incomplete polymer extension.

In an attempt to estimate the degree of stretching around a stagnation point, Menasveta and Hoagland have performed light scattering experiments. They claim to show a molecular extension ratio of approximately two[32]. However, the authors admit that the interpretation of their results is not straightforward. Furthermore,

as pointed out by Larson *et al.*, such a picture would be completely incompatible with the directly observed extension of DNA[30].

Batcheder and Cooper have tried to estimate the molecular stresses in the stretched molecule around a stagnation point directly by the use of Raman spectroscopy[33]. The application of stress will result in shifts in the Raman bands associated with the polymer chain. The Raman shifts and corresponding stresses reported were modest compared to those expected for a fully stretched molecule, which has led these authors to suggest a 'kinked' molecular conformation of one third of the overall extended length[33]. However, the solutions used were not in the dilute regime. Mechanical fracture was noted in this study and was well accounted for by the TABS theory—but this requires the molecules to be extended in apparent contradiction to the 'kinked' conformation. In any case, it should be recalled that the Hinch 'kink' model is inappropriate for such flow regimes.

In this paper we report new experimental studies into the stretching of dilute solutions in extensional flows. We introduce new techniques for the control of flow, retardation measurement and the absolute determination of birefringence and induced molecular orientation. These observations are correlated with simultaneous extensional viscometry, so that the magnitude and molecular origin of extensional viscosification can be directly observed. In a following paper we extend the work to include detailed modelling of the flow-field together with a comparison of the evolution of molecular and fluid strain[34].

EXPERIMENTAL

To a first approximation, the flow field created by sucking fluid into two opposed jets can be considered to be uniaxial extension with a nominal strain rate, $\dot{\epsilon}_{nom}$, at volume flow rate, Q, defined as[16,17,19]:

$$\dot{\epsilon}_{\text{nom}} = \frac{Q}{Ad} \tag{1}$$

where A is the area of each jet and d is the jet separation. A pure uniaxial extensional flow would have a constant strain rate throughout.

Apparatus

The opposed jets system allows simultaneous optical birefringence and flow resistance measurements, enabling the correlation of molecular orientation with its effect upon the flow field[19].

A linear CCD (Charged Coupled Device) array was introduced, aligned along the symmetry plane, in order to record the intensity profiles across the birefringent lines. This detector provides line width measurements and more significantly, allows *true* birefiringence profiles to be extracted from the retardation projections. The determination of the proportion of the stretching zone containing highly extended molecules, allows a better assessment of their contribution to the observed extensional viscosity increase.

Odell *et al.* described the modification of a vacuum driven apparatus to include simultaneous flow resistance measurements, by monitoring the pressure drop across the jets (ΔP)[19]. These data are used to determine effective extensional viscosities.

A new 'pressurized' system has been introduced in order to extend the available strain rate range. The practical arrangement for the pressurized apparatus is shown in *Figure 1*. The solution reservoir, flow cell, piston pump and pipework are constructed from stainless steel, and are joined together with Swagelok connectors.

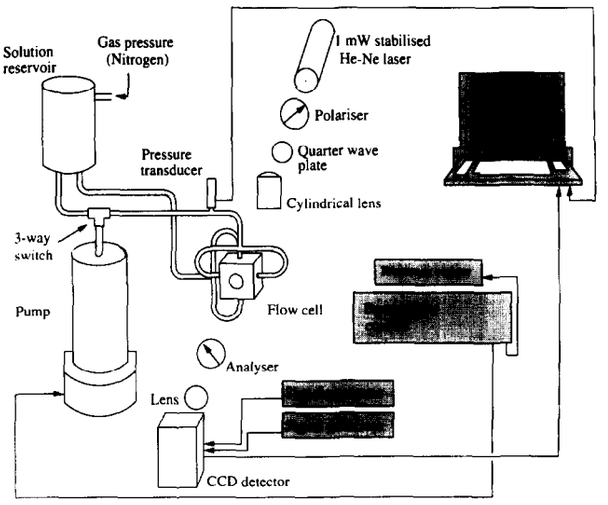

Figure 1 Schematic diagram of the apparatus used with the opposed jets for measurement of extensional birefringence and flow resistance (pressurized system)

Polymer solution in the reservoir is forced under pressure [typically 3 atmospheres from the nitrogen (N_2) cylinder], through the flow cell, which contains two solution inlets to provide a symmetrical inlet flow. Suprasil glass was used for the windows, because of the low void content. The jets in this cell (termed 'metal jets') had a diameter of 0.6 mm and a separation of 0.35 mm. The polymer solution exits the flow cell, via the jets and flows into the receiving piston pump, which is stepper motor controlled. This arrangement enables the pressure in the cell to remain constant, avoiding problems of changing residual window birefringence. The strain rate range available is approximately 5–60 000 s^{-1}. [Some of the experimental measurements detailed in the Results section were made using a vacuum driven apparatus, with a glass flow cell. The jets in this cell (termed 'glass jets') had a diameter of 0.35 mm and a separation of 0.57 mm].

Birefringence observation and measurement

The optical train for birefringence observation is also shown in *Figure 1*. Illumination of the extending region between the jets is provided by a 1 mW Renishaw stabilized He–Ne laser ($\lambda = 632.8$ nm). The use of a stabilized laser is critical for reliable measurements. The laser beam was focused down to pass between the jets, such that the resulting beam diameter was still large enough to span the region of extension, typically the peak width at half height was 200 μm. The beam was centred as precisely as possible on the stagnation point. The use of a cylindrical lens to further focus the horizontal direction gives an even greater illuminating intensity, and this method has been found to be particularly useful for projecting the signal onto the linear CCD array. Residual birefringence (e.g. from the cell windows) was removed with a Sénarmont compensator.

Relationship between measured intensity and retardation. Riddiford and Jerrard have developed a linear retardation detection method which provides significant advantages compared to the traditional quadratic technique, as well as giving a better signal-to-noise ratio[35]. Their method involves observing the birefringent signal with a $\lambda/4$ plate between slightly uncrossed polars.

The intensity of the birefringent signal, I_s is given by:

$$I_s = \frac{I_o}{4}\delta_1^2 + \frac{I_o}{2}\delta_1 S + \frac{I_o}{4}S^2 \qquad (2)$$

where I_o is the intensity of the incident beam, δ_1 is a constant retardation (background) signal due to the uncrossing of the polars and S is the sum of all the signals due to birefringent elements in the system. The first term (large and constant) can be subtracted from the total signal, leaving a term linear in S and an S^2 term. By ensuring δ_1 is made large in comparison to S, the S^2 term may be neglected, which leaves I_s proportional to S. This condition is satisfied practically by uncrossing the polars to give a background intensity ($I_o\delta_1^2/4$) of $\approx$10–20 times the quadratic I_s signal.

Practical techniques for birefringence observation

Images of the birefringent region can be observed and recorded through a microscope, with crossed polars. For a more detailed analysis, a detection system providing information about line widths and local intensity variations across the birefringent region would be required. This may be achieved by scanning a sharply focused beam across the birefringent line and using a photodiode or photomultiplier tube (PMT) to record intensity as a function of position. The retardation profiles are then fitted to a Gaussian distribution, which can be analytically Abel transformed to yield the radial distribution of birefringence. Fuller and Leal[21], and Cathey and Fuller[20] have used this method in the four-roll mill and opposed jets respectively, with the Fast Polarization Modulation (FPM) technique for improved sensitivity in the measurement of retardation. They report profiles that are approximately Gaussian in shape. Focussed laser scanning coupled with FPM and the use of the Abel transform has also been used by Nguyen *et al.*[31].

However, this method has drawbacks. Mechanical scanning means that an instantaneous observation of the whole flow field is not possible. The deconvolution procedure contains uncertainties, since the laser beam profile must be estimated, and this results in reduced resolution. Since Fuller and Leal[21] used a width of between 30 and 50% of the deconvoluted line width, such errors may be considerable, although it would be of less significance for Cathey and Fuller[20], who used a beam width $\approx$6% of the line width. This sharp focusing of the beam means that it is non-parallel as it passes through the birefringent region, adding further complexity to the resultant signal analysis. Cathey and Fuller did not discuss this point. Even when the laser is relatively narrow compared to the line width, it may significantly modify the resulting profiles when the line is non-Gaussian due to flow perturbation. The relevance of this to the results of Nguyen *et al.* has been discussed by Carrington and Odell[36].

The CCD array. An alternative to the scanning method is the direct imaging technique, which uses a stationary detector containing many independent segments measuring the incident light intensity. If an image of the birefringent line is focused onto the plane of such a detector, line profiles may be digitally recorded. A linear charge coupled device (CCD) pixel array was employed for this work. The CCD array used was a model TH 7806(Z), manufactured by Thomson-CSF. The linear array consists of 256 light sensitive pixels, each one of dimensions 13 μm × 13 μm. The two clock pulse trains, for the integration (10 Hz) and readout (25 kHz) clocks, were supplied externally.

Processing of the CCD traces. The CCD data are subsequently processed to subtract the background and normalize by the laser beam profile to yield a true retardation profile.

Height and width parameters from the retardation peaks can be measured easily, to obtain information that has been previously unavailable from photodiode measurements. However, *birefringence* profiles create the greatest interest, as they yield information specific to molecular conformation. The retardation intensity is also a function of the path length, z, through the sample. In the 3-dimensional axisymmetric flow field of the opposed jets, z is a function of (vertical) distance, y, from the symmetry axis and Δn is a function of the radial distance, r. The CCD recordings of the retardation profiles can be considered as edge-on projections of a thin circular slice of the birefringent region. The true birefringence profile, $\Delta n(r)$, is obtained from these retardation profiles by using a transformation routine.

The retardation–birefringence transform

The use of the Abel transform poses acute problems. As discussed above, previous workers have fitted a Gaussian distribution which enables an analytical solution to the transform[20,31]. The solution proves to be trivial however. The abel transform of a Gaussian is simply a Gaussian of the same width, thus the retardation Gaussian is simply the integral of the birefringence Gaussian. This reduces the Abel transform to the simple result $B = R/r_o\sqrt{2\pi}$, where B is the peak (central) birefringence, R is the peak retardation and r_o is the width of the Gaussian distribution. With experimental uncertainty, this is little more than the long standing practice of dividing the retardation by the line width[16,36]. Furthermore, as will be shown later, the assumption of a Gaussian fit is seriously flawed. For these reasons, a numerical technique which can transform cylindrically symmetric profiles of arbitrary shape, has been used in this work.

The birefringent region is considered to consist of thin concentric annuli, each of constant birefringence (Δn). The value of $(\Delta n)_i$ has to be determined for each annulus, A_i. A numerical method must then be used to derive $\Delta n(r)$ from the measured retardation profile, because the form of the function $\Delta n(r)$ is unknown. The thickness of each annulus is defined to be the width which is covered by a single CCD pixel[24,37].

By an iterative procedure, the true birefringence profile is generated. The data used are folded and averaged around the central pixel due to the required cylindrical symmetry. Tatham has assessed the performance of the iteration procedure by using a noise-free

Gaussian test function, and found the error in $(\Delta n)_{max}$ to be 0.69% and that in $(\Delta n)_{width}$ to be 0.64%[37].

Calibration of the CCD traces

In order to convert the CCD traces to retardation and birefringence, two calibrations have to be undertaken. The calibration of true distance, y (μm), in the vertical plane of the jets *versus* pixel width is facilitated by monitoring the translation of the cell on its micrometer mountings. The CCD voltage can be calibrated in terms of retardation against a $\lambda/30$ plate.

The uncertainty levels in the voltage readings give a combined error in R of approximately $\pm$ 5%. This factor, in combination with the reproducibility of results in this study, allows some confidence to be placed in the calibration method.

Flow resistance measurements: effective extensional viscosity

Newtonian fluids. For a Newtonian fluid in a uniaxial extensional flow field, the pressure drop, ΔP_{ext}, due to viscous dissipation is given by:

$$\Delta P_{ext} = \eta_e \dot{\epsilon} \tag{3}$$

where $\dot{\epsilon}$ is the nominal extensional strain rate and η_e is the extensional viscosity of the fluid. In a Newtonian fluid, η_e is independent of $\dot{\epsilon}$ and for this flow geometry, the extensional viscosity is given as:

$$\eta_e = 3\eta_s \tag{4}$$

where η_s is the Newtonian shear viscosity. The factor of 3 is the Trouton ratio for this geometry.

Extensional viscosity values for any fluid can be obtained by using equation (3), and measuring ΔP_{ext} *versus* strain rate.

The measured values of the pressure drop across the jets include contributions from other sources, in addition to ΔP_{ext}. Therefore, this technique can only be used to yield an *effective* extensional viscosity, η_e', and to allow a comparison of the behaviour of Newtonian solvents with non-Newtonian polymer solutions.

Flow resistance measurements made for the aPS solutions should allow comparisons to be made with theoretical expectations for the increase in extensional viscosity due to stretched molecules, which is predicted to depend upon N to the power 1 to 3[13,14]. An assessment must be made of the effective area over which molecules experience significant extension, since a measured ΔP value will be dependent on this. Significant molecular extension is confined to a narrow region surrounding the stagnation point. The birefringence profiles obtained using the CCD detector allow an analysis of this region to be made.

For a Newtonian fluid in the opposed jets, a plot of ΔP against $\dot{\epsilon}$ would be linear, if the measured ΔP was equivalent to ΔP_{ext} in equation (3). However, ΔP *versus* $\dot{\epsilon}$ curves for solvents have been found to exhibit curvature, which implies that there is a contribution to ΔP from other factors[38].

The curvature has been attributed to the Bernoulli effect due to convergent flow, which introduces a term in $\dot{\epsilon}^2$ into the equation for ΔP, such that:

$$\Delta P = B\dot{\epsilon} + C\dot{\epsilon}^2 \tag{5}$$

where B and C are constants, and this correlates well with experimental data[38].

Tatham used mixtures of isopropanol and water to systematically vary the viscosity and showed that the quadratic contribution was not related to viscosity, but is inertial in origin (since the fluid density remains approximately constant)[37].

The inertial contribution to ΔP is expected to be of similar magnitude in solvent and dilute polymer solutions, due to its dependence on density and not viscosity. Therefore, the value of C derived from the solvent curves (equation (5)) can justifiably be used to calculate the inertial contribution, $\Delta P_I (\equiv C\dot{\epsilon}^2)$, for all ΔP *versus* $\dot{\epsilon}$ curves (i.e. for both solvent and polymer solutions).

The subtraction of the ΔP_I contribution from the curved ΔP *versus* $\dot{\epsilon}$ solvent trace results in a linear plot. This 'corrected' plot incorporates not only ΔP_{ext} (equation (3)), but also contributions from shear flows between the points of measurement, such as Poiseuille flow inside the jets. All shear contributions may be combined into a single term (ΔP_S), which will be linear in $\dot{\epsilon}$.

The extensional viscosity of a Newtonian liquid in the opposed jets may be calculated using the approximation:

$$\eta_e \approx \frac{(\Delta P - \Delta P_I - \Delta P_S)}{\dot{\epsilon}} \tag{6}$$

For water, the value obtained ($\eta_e \approx 0.9$ Pa s) was more than two orders of magnitude greater than the expected value of three times the shear viscosity (0.003 Pa s). The reason for this difference remains to be completely explained. Part of the explanation is that the flow field simulations of the opposed jets have shown that the developed flow field is not perfect uniaxial extension[34]. Therefore, the strain rate is not precisely given by equation (1), nor is it entirely uniform in the region between the jets. This overestimates the value of η_e by less than one order of magnitude, which still provides a measured value much larger than the actual value. Tatham has also shown that different jet geometries give significantly different values of the apparent extensional viscosity of water[37].

Fuller *et al.* have measured extensional viscosities at low Reynolds numbers in highly viscous solvents[39]. Values of $(\eta_e)_{solvent}$ have been derived from the force required to maintain constant separation of pivoted jets, and are reported as being close to theoretical expectations.

Non-Newtonian fluids. Experiments using high molecular weight polymers in low viscosity solvents (in fixed jet systems) show that the increase in ΔP compared to pure solvent is much higher than can be accounted for by the increase in shear viscosity (at least above $\dot{\epsilon}_c$). Accordingly, as a first order approximation (and neglecting the shear contribution ΔP_S), the slope of the linear $(\Delta P - \Delta P_I)$ against $\dot{\epsilon}$ plot generates a parameter proportional to (and dominated by) the extensional viscosity. This is defined as the 'effective extensional viscosity', η_e':

$$\eta_e' = \frac{d(\Delta P - \Delta P_I)}{d\dot{\epsilon}} \tag{7}$$

Note that at the highest strain rates, the experimental ΔP *versus* $\dot{\epsilon}$ curve may show a discontinuity from the quadratic behaviour described by equation (5). This has been attributed to the development of turbulent flow[37].

By applying a quadratic curve fit to the ΔP *versus* $\dot{\epsilon}$ trace, the constants B and C of equation (5) can be obtained. The ΔP_I component ($\equiv C\dot{\epsilon}^2$) can then be subtracted from the ΔP *versus* $\dot{\epsilon}$ trace of the polymer solution, to give the excess pressure difference due to the polymer as:

$$(\Delta P)_{pol} - (\Delta P_I) = (\eta_e')_{pol}\dot{\epsilon} \tag{8}$$

Differentiating equation (8) gives a first approximation to the effective excess extensional viscosity due to the polymer $(\eta_e')_{pol}$:

$$\frac{d}{d\dot{\epsilon}}\left((\Delta P)_{pol} - (\Delta P_I)\right) = (\eta_e')_{pol} \tag{9}$$

The linear coefficient, B, is then used to calibrate $(\eta_e')_{pol}$, since B is related to $(\eta_e')_{solvent}$. This provides a definition of the relative effective extensional viscosity, $(\eta_e')_r$:

$$(\eta_e')_r = \frac{(\eta_e')_{pol}}{B} \tag{10}$$

A definition of an effective intrinsic extensional viscosity, $[\eta_e']$, for data obtained from the opposed jet apparatus, is therefore given as:

$$[\eta_e']_{c\to 0} = \frac{(\eta_e')_r - 1}{c} \tag{11}$$

where c is the concentration in g ml^{-1}. A value for the normalized extensional viscosity (the increase in extensional viscosity due to stretched molecules), H, for dilute solutions, can be obtained by using the above expression combined with:

$$H \approx \frac{[\eta_e']}{3[\eta]} \tag{12}$$

It can be seen that the subtraction of the quadratic ΔP_I contribution from the polymer solution data should provide relative values for $(\eta_e')_{pol}$, and deviations from Newtonian $(\eta_e')_{solvent}$ behaviour will be clearly illustrated. Note that if flow field modification occurs due to the stretching molecules, then the ΔP_I contribution will be altered, and the subtraction of the quadratic component is not entirely valid.

Therefore, $(\eta_e')_{pol}$ curves are a qualitative assessment of the extensional viscosity behaviour of polymer solutions, and can only be used to compare trends and give order of magnitude estimates for the normalized extensional viscosity. The extensional viscosity of the polymer should be examined in the laminar flow regime of the solvent, and in the absence of any flow modification.

The opposed jet apparatus does, however, offer the unique possibility of assessing a parameter which is dominated by the extensional viscosity, which can then be directly correlated with observation of molecular extension.

Solution preparation

The aPS samples used in these experiments were closely monodisperse (polydispersity index = 1.05–1.2), supplied by Polymer Laboratories. Decalin is a θ solvent for aPS close to room temperature, and has a viscosity of 0.0024 Pa s at 20°C. TCP is a good solvent for aPS at room temperature[40], and the commercial mix of isomers was found to have a viscosity of 0.051 Pa s at 23°C. The increased viscosity of TCP, compared to decalin, would be expected to reduce inertial effects in the flow field. The PEO sample used had a peak molecular weight, $M_p = 1.39 \times 10^6$, and was closely monodisperse, with $M_w/M_n = 1.15$. The sample was supplied by Polymer Laboratories. For the relevant molecular weight range, the Mark–Houwink exponent, $a = 0.76$[41].

The lower viscosity solvents were filtered through a 2 μm filter at room temperature. The polymer powder was slowly added onto the surface of the filtered solvent, whilst stirring vigorously with a magnetic stirrer, to create a vortex. After dispersion of the polymer, the stirring was reduced to a minimum to avoid any possibility of mechanical degradation. The solution process was allowed to proceed for between 2 and 7 days, depending on the concentration and the polymer–solvent combination. Highly dilute solutions were prepared from a mother solution of typically five times the desired concentration.

In order to make up solutions of aPS polymer in the highly viscous tricresyl (tolyl) phosphate (TCP), the polymer was first dissolved in a small quantity of dichloromethane. The dichloromethane solution was dispersed into the TCP and dry N_2 gas was then passed above this mixture, in order to remove the dichloromethane by evaporation.

RESULTS AND DISCUSSION

Retardation and birefringence profiles

Dilute solution investigations were started at a concentration of 0.02%, which for the molecular weight range used, was well below the onset concentration for intermolecular entanglements in the opposed jets[38].

Flow field perturbation: screening effects. The change in retardation and birefringence profiles with strain rate, for a 0.02% $M_p = 8 \times 10^6$ aPS/decalin solution in the glass jets geometry, is shown in *Figure 2*. As the strain rate increases, the retardation profiles increase in height and width. However, the CCD profiles show detail which has not been previously available from other detection methods. As the strain rate increases, the initial peak profile of the retardation traces starts to develop a flat top. The retardation profile at $\dot{\epsilon}_{nom} = 5500\,s^{-1}$ has steep sides leading to a substantial plateau, indicating an almost 'block-like' area of retardation. A further increase in strain rate causes the flat tops of the retardation profiles to evolve into a central dip.

The application of the retardation-birefringence transform changes the peak shapes only slightly at low $\dot{\epsilon}_{nom}$. However, at higher values of $\dot{\epsilon}_{nom}$, the transform of a flat-topped retardation profile gives rise to a birefringence profile with a dip in the middle (e.g. at $\dot{\epsilon}_{nom} = 4500\,s^{-1}$). This effect arises because central points have accumulated retardation over longer optical path lengths than the outer points and thus, the achievement of constant retardation on approach to the centre, means that the central birefringence must drop. When the retardation profiles themselves begin to exhibit a central dip (with continuing $\dot{\epsilon}$ increase), the corresponding dip in the birefringence profiles becomes very deep. The dark central line, or 'pipe', in the birefringent line could be viewed by removing the CCD detector and replacing it with a microscope. Müller has used similar samples to obtain pipe structures in the opposed jets, but they were not found at such low concentrations[38].

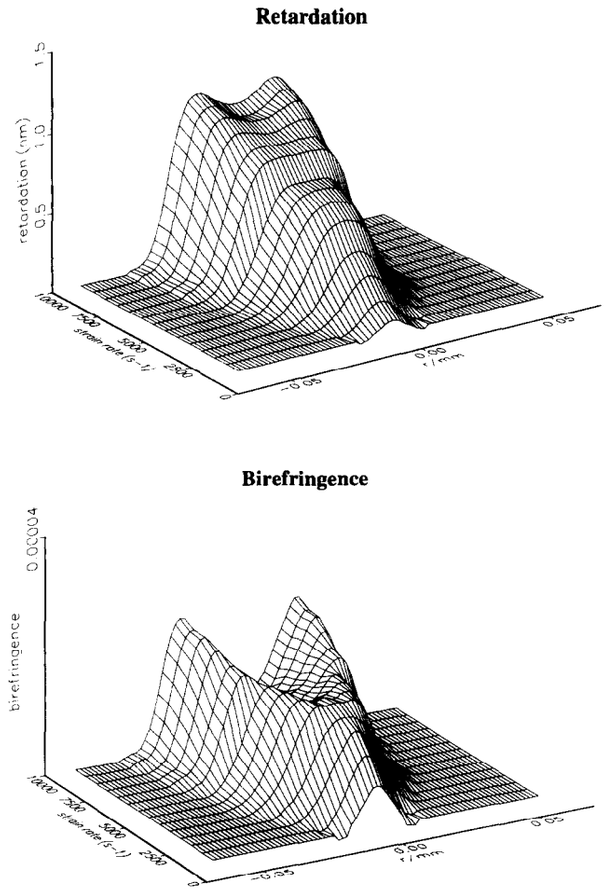

Figure 2 The development of the retardation and birefringence profiles with strain rate, for a 0.02% $M_p = 8 \times 10^6$ aPS/decalin solution (glass jets apparatus). $r = 0$ is the stagnation point

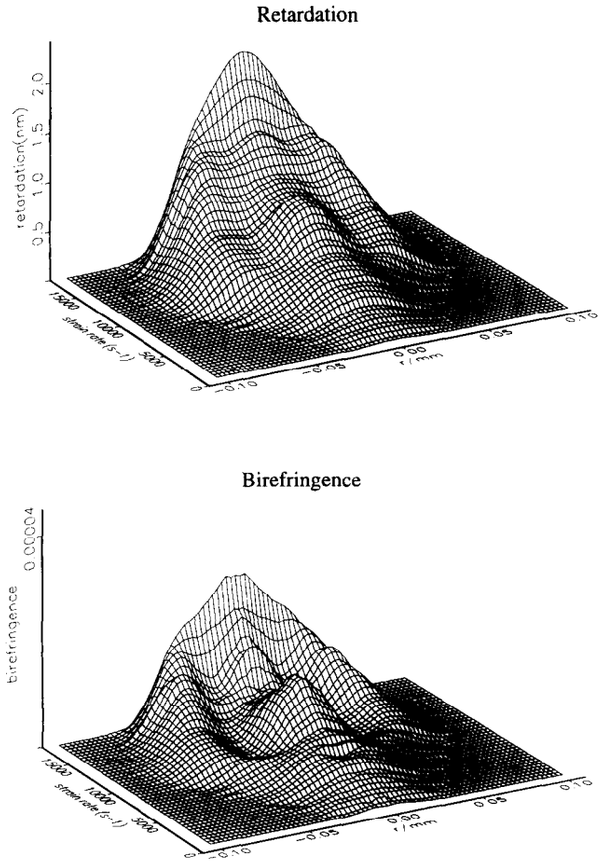

Figure 3 The development of the retardation and birefringence profiles with strain rate, for a 0.02% $M_p = 8.5 \times 10^6$ aPS/decalin solution (metal jets apparatus). $r = 0$ is the stagnation point

A drop in Δn at the centre of the lines implies a reduction in chain extension, which in turn suggests that the molecules (in the centre of the birefringent zone) are no longer experiencing sufficient strain rate to remain fully stretched. Ng and Leal have recently highlighted the effects of concentration upon the development of birefringence around the stagnation point of the two roll mill[42]. Velocimetry shows directly the perturbation of the flow-field by the stretching molecules. They report reductions in birefringence greater than would be expected on the basis of flow-perturbation alone, and suggest the effect arises from entanglements. Harlen *et al.* have studied the flow modification near a stagnation point using a FENE (finitely extensible non-linear elastic) dumb-bell model *with non-linear hydrodynamic friction*[43]. They predict that pipe structures can occur at dilute polymer concentrations without direct mechanical interactions between neighbouring molecules. The process of chain extension is expected to generate massive extensional viscosities in localized regions, with an accompanying reduction in local flow velocity. Odell *et al.* have verified this effect experimentally in semi-dilute solution (0.2% $M_w = 4 \times 10^6$ aPS/decalin), but found no flow modification for a dilute (0.03%) solution of the same sample[19]. However, this was probably due to resolution limitations of the velocimetry technique used.

Computer simulations have shown that differences can be expected in the flow fields generated by the two jet geometries used in the experiments[34]. The retardation and birefringence profiles for a 0.02% $M_p = 8.5 \times 10^6$ aPS/decalin solution in the metal jets geometry are shown in *Figure 3*. It is again obvious that severe modification of the flow field is taking place, but the screened profiles are markedly different from those obtained in the glass jets. The outstanding feature here is the 'pipe-within-a-pipe' (i.e. at $\dot{\epsilon}_{nom} = 8300\,s^{-1}$, the retardation and birefringence profiles show three peaks of equal intensity). This structure has been visually observed by Müller[38], but at concentrations in the semi-dilute regime. The FENE dumb-bell with non-linear hydrodynamic friction model of Harlen *et al.*[43] cannot provide an extension rate near the centre line which increases again, after dropping below the stretch–coil transition value and hence, more complex structures seen in experiments (e.g. a 'pipe-within-a-pipe') are not predicted.

Unperturbed flow at low concentration. In order to assess the consequence of dilution on the observed flow modification effects, a 0.01% $M_p = -8.5 \times 10^6$ aPS/decalin solution was analysed in the metal jets, and the retardation and birefringence profiles are shown in *Figure 4*. The comparison of *Figure 4* with *Figure 3* (0.02% solution of the same polymer) is striking. The retardation profiles for the 0.01% solution show a single peak, which increases in height and width up to $\dot{\epsilon}_{nom} \approx 6500\,s^{-1}$. At this point (and up to $\dot{\epsilon}_{nom} \approx 9000\,s^{-1}$), there is evidence of some flat-tops on the peaks, and a slowing down

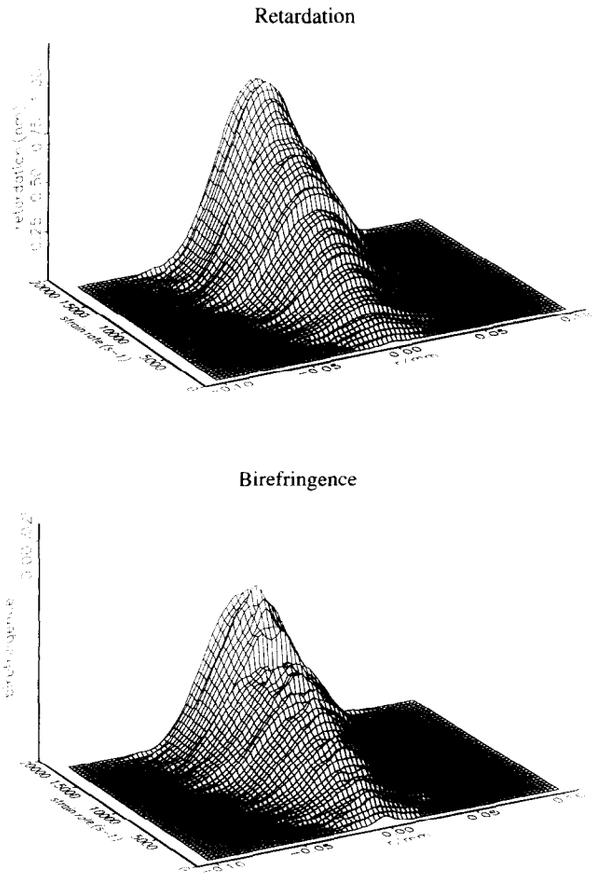

Figure 4 The development of the retardation and birefringence profiles with strain rate, for a 0.01% $M_p = 8.5 \times 10^6$ aPS/decalin solution (metal jets apparatus). $r = 0$ is the stagnation point

in the rate of intensity increase with strain rate. The retardation profiles show an intensity plateau at $\dot{\epsilon}_{nom} \approx 11\,000\,s^{-1}$ and a slight reduction in width at strain rates beyond this. The associated birefringence profiles mirror the above trend and show a levelling off of intensity at $\dot{\epsilon}_{nom} \approx 6000$–$8500\,s^{-1}$, with the profiles exhibiting flattened tops and relatively minor central dips. A single peak is recovered at $\dot{\epsilon}_{nom} \approx 9000\,s^{-1}$, which proceeds to plateau in intensity ($\dot{\epsilon}_{nom} \approx 10\,000\,s^{-1}$). The overall picture is of greatly reduced flow modification compared to the 0.02% solution, which appears to manifest itself only in the region of $\dot{\epsilon}_{nom} \approx 6000$–$9000\,s^{-1}$.

A plot of maximum birefringence (Δn_{max}) *versus* strain rate ($\dot{\epsilon}$) for the 0.01% solution is shown in *Figure 5*, and this gives an indication of the amount of material stretching. The maximum birefringence levels off in the region where modification of the flow field appears to take place, and then recovers to plateau at higher strain rates. The plateau value of $\Delta n_{max} = -(1.62 \pm 0.02) \times 10^{-5}$.

Molecular weight changes. The effect of a reduction in molecular weight on the flow behaviour is shown in *Figure 6*, which details the retardation and birefringence profiles for a 0.01% $M_p = 4 \times 10^6$ aPS/decalin solution in the metal jets. The single peak nature of the profiles throughout the strain rate range is very clear. *Figure 7* shows the Δn_{max} *versus* $\dot{\epsilon}$ plot for this solution. The plateau in birefringence occurs at a strain rate of $\dot{\epsilon}_{nom} = 20\,000\,s^{-1}$, corresponding to a value of

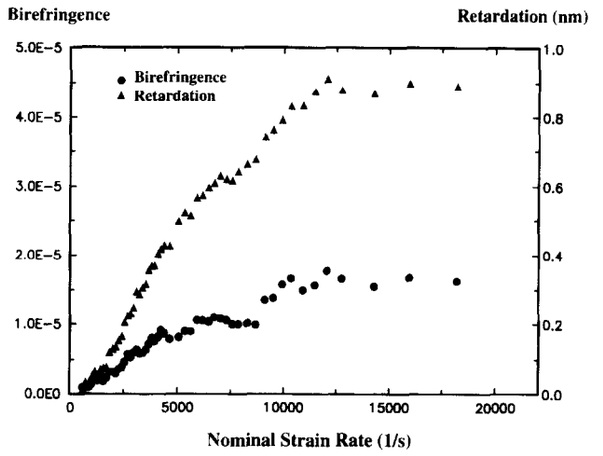

Figure 5 Maximum birefringence (●) and maximum retardation (▲) plotted against nominal strain rate, for a 0.01% $M_p = 8.5 \times 10^6$ aPS/decalin solution (metal jets apparatus)

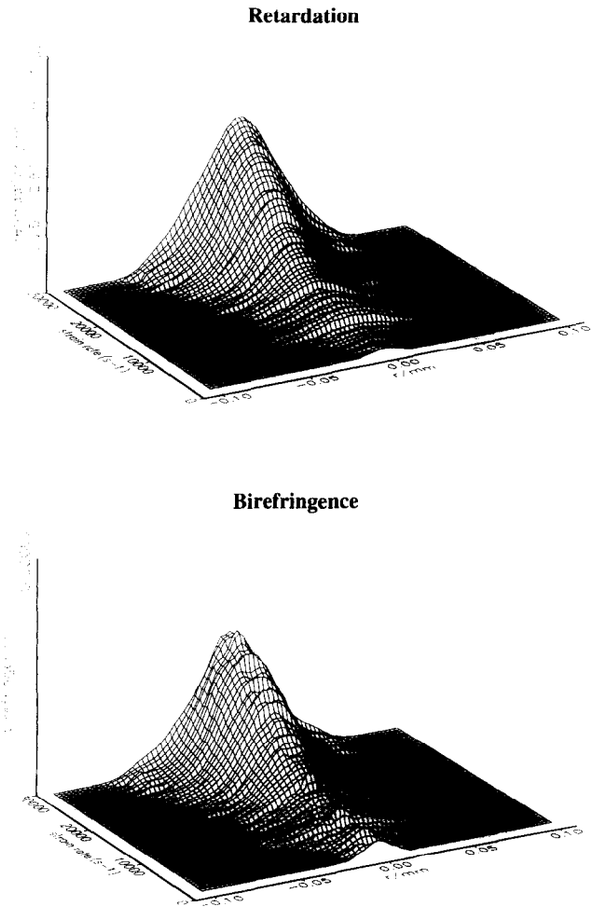

Figure 6 The development of the retardation and birefringence profiles with strain rate, for a 0.01% $M_p = 4 \times 10^6$ aPS/decalin solution (metal jets apparatus). $r = 0$ is the stagnation point

$\Delta n_{max} = -(1.12 \pm 0.02) \times 10^{-5}$. The increase of Δn_{max} in this case appears to be smoother than the curve for the 0.01% $M_p = 8.5 \times 10^6$ aPS/decalin solution (*Figure 5*), which may be indicative of a reduction in flow modification (to almost zero) at this molecular weight. The occurrence of flow modification (indicated by changes in the retardation and birefringence profiles) has been shown

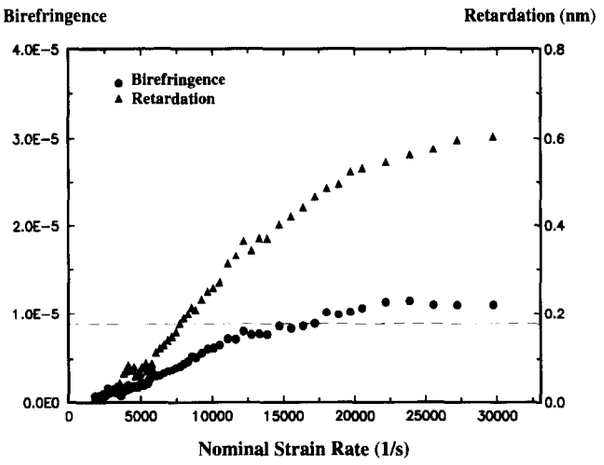

Figure 7 Maximum birefringence (●) and maximum retardation (▲) plotted against nominal strain rate, for a 0.01% $M_p = 4 \times 10^6$ aPS/decalin solution (metal jets apparatus). The dashed line shows an estimate of the maximum theoretical birefringence value for fully stretched molecules

to coincide with a levelling-off, or dip, in the Δn_{max} *versus* $\dot{\epsilon}$ curve. The decrease in magnitude of such discontinuities with a lowering of molecular weight and concentration, culminating with the relatively smooth profiles and maximum birefringence plot of the 0.01% $M_p = 4 \times 10^6$ aPS/decalin solution, suggests that this result is showing 'truly dilute' behaviour in the flow field, i.e. modification of the flow field due to polymeric additives appears to be absent. It is notable that the concentration required to see such truly dilute behaviour is of the order of $c^*/100$, depending upon the method of estimation of c^*.

The use of two lower molecular weight samples ($M_p = 3 \times 10^6$ and $M_p = 1.9 \times 10^6$) at a concentration of 0.01% has confirmed the production of single peak profiles throughout the strain rate range, and also the attainment of a plateau birefringence.

Figure 8 shows the birefringence as a function of strain-rate for the 0.01%, $M_p = 1.9 \times 10^6$ aPS (filled squares). The solid line in *Figure 8* represents a simulated transition, assuming perfect criticality and that strain-rate scales as $M^{-1.5}$, derived from the cumulative molecular weight distribution as assessed by g.p.c. Clearly the width of the transition is fully accounted for by the residual polydispersity of the sample.

Solvent quality. The effect of solvent quality improvement has been assessed by analysing a 0.005% $M_p = 8.5 \times 10^6$ aPS/TCP solution, and the measured retardation and birefringence profiles are shown in *Figure 9*. At the lowest measured strain rate ($\dot{\epsilon}_{nom} = 35\,s^{-1}$), the retardation profile is 'block-like', i.e. the profile has relatively steep sides leading to a substantial plateau region. As the strain rate increases, this profile is essentially maintained and grows in both height and width. Over the strain rate range of approximately 160–200 s^{-1}, the retardation profile appears to recover to a more Gaussian approximation, but this is short-lived, and a block-life profile reappears after $\dot{\epsilon}_{nom} \approx 200\,s^{-1}$. The application of the retardation-birefringence transform creates birefringence profiles which have steep sides and a wide central region containing a dip. This profile is

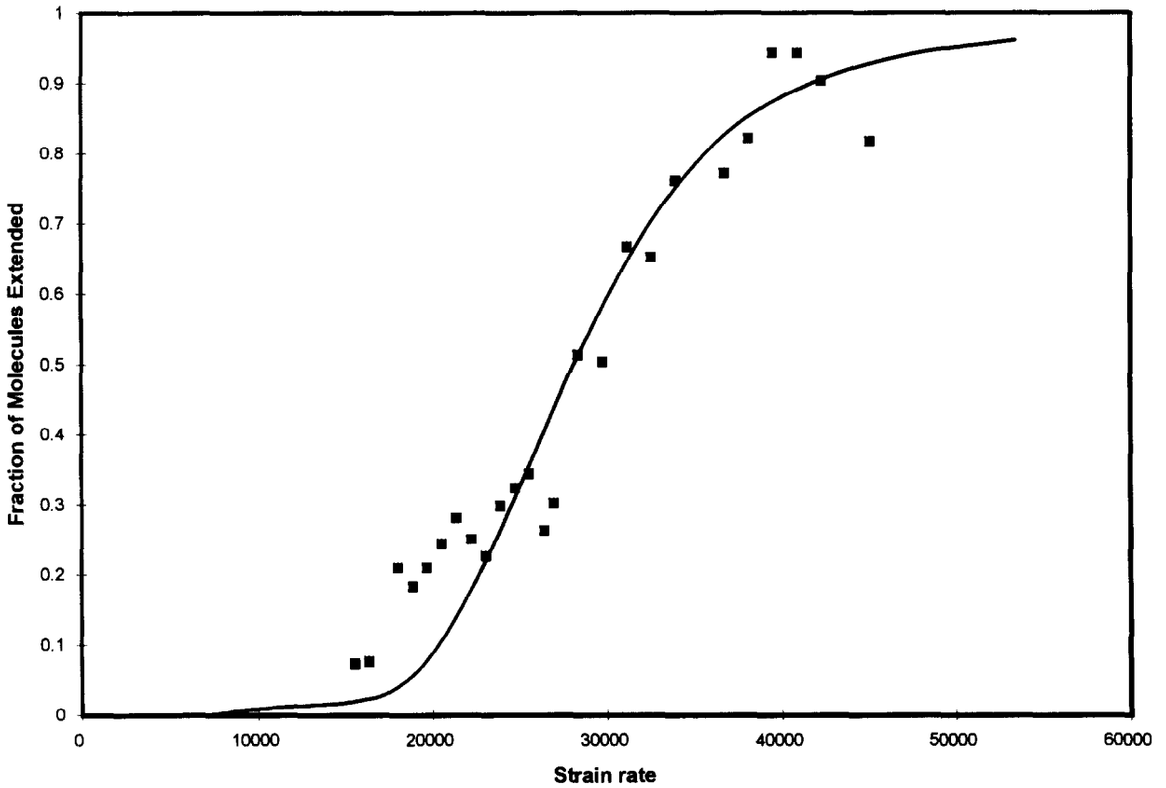

Figure 8 The fraction of molecules extended as assessed from the maximum birefringence data (■) plotted against nominal strain rate, for a 0.01% $M_p = 1.9 \times 10^6$ aPS/decalin solution (metal jets apparatus). The solid line represents a simulated transition derived from the cumulative g.p.c. trace (courtesy of Polymer Laboratories)

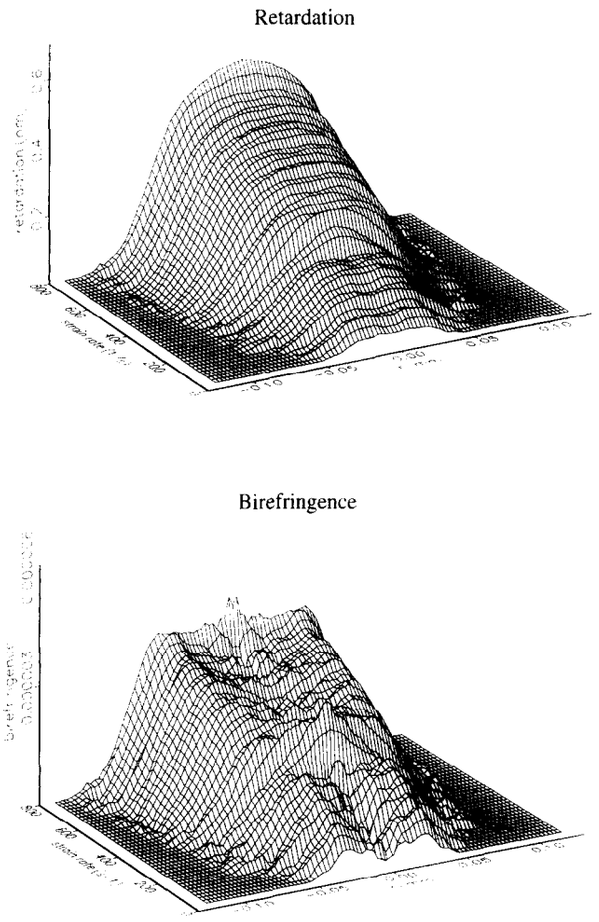

Figure 9 The development of the retardation and birefringence profiles with strain rate, for a 0.005% $M_p = 8.5 \times 10^6$ aPS/TCP solution (metal jets apparatus). $r = 0$ is the stagnation point

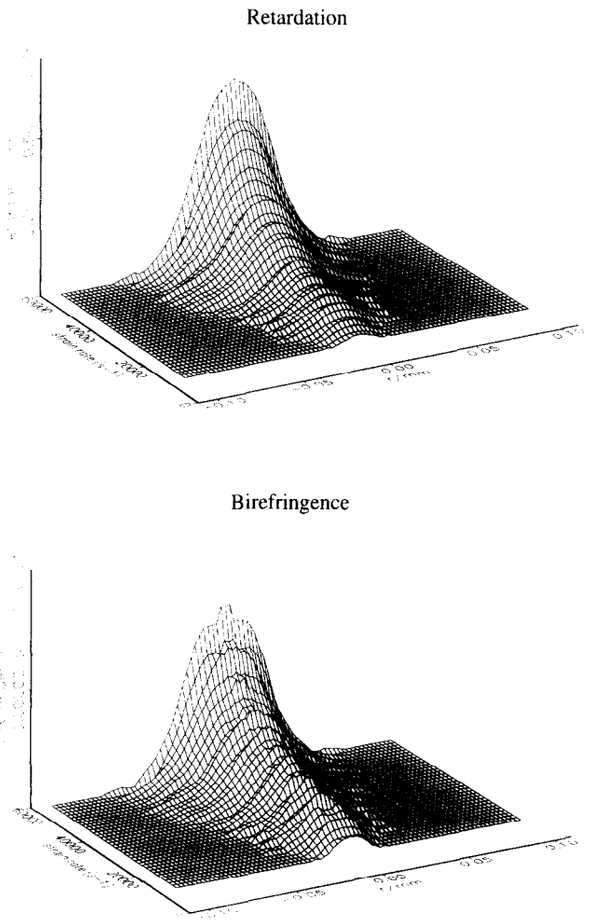

Figure 10 The development of the retardation and birefringence profiles with strain rate, for a 0.02% $M_p = 1.39 \times 10^6$ PEO/water solution (metal jets apparatus). $r = 0$ is the stagnation point

disrupted in the region of $\dot{\epsilon}_{nom} = 160$–$200\,s^{-1}$, where a single peak is recovered.

The retardation and birefringence profiles appear to suggest that throughout the measured strain rate range, the flow field is subject to modification by the extending polymer molecules, even for this highly dilute solution. Note that the width of the region of significant molecular extension is greater in TCP than in decalin, for an equivalent polymer.

A study of dilute poly(ethylene oxide) (PEO) solution in distilled water ($\eta_s = 0.001$ Pa s), which is regarded as a good solvent near room temperature (23°C), was undertaken in order to assess the extensional flow behaviour of another highly flexible polymer. *Figure 10* shows the change in the retardation and birefringence profiles with strain rate for a 0.02% $M_p = 1.39 \times 10^6$ PEO/water solution. The retardation profiles are seen to increase in height and width over the measured strain rate range. The profile remains a single peak, of approximately Gaussian nature, throughout, which appears to indicate an absence of any major flow modification effects. The birefringence transform also produces a single peak.

Figure 11 is a plot of Δn_{max} *versus* $\dot{\epsilon}$, for the PEO/water solution. From these data, it is difficult to determine whether Δn_{max} is tending to a plateau at the highest strain rates measured (but note that there appears to be no sign of saturation in the retardation data). At $\dot{\epsilon}_{nom} = 59\,000\,s^{-1}$, the value of $\Delta n_{max} = 0.96 \times 10^{-5}$.

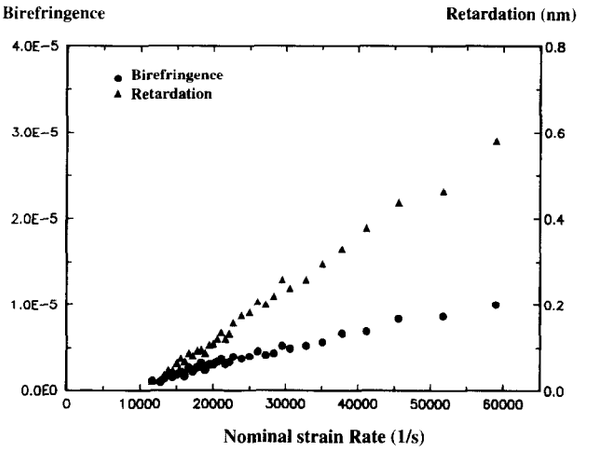

Figure 11 Maximum birefringence (●) and maximum retardation (▲) plotted against nominal strain rate, for a 0.02% $M_p = 1.39 \times 10^6$ PEO/water solution (metal jets apparatus)

Theoretical calculations of Δn_0

The intrinsic birefringence of a fully stretched

molecule, Δn_o may be calculated by using the following equation[44,45]:

$$\Delta n_o = \frac{2\pi(n_o^2+2)^2}{n_o}\frac{N_A c}{N_{m/s} m}(\alpha_1 - \alpha_2) \quad (13)$$

where n_o is the mean refractive index of the polymer, N_A is Avogadro's number, c is the concentration, $N_{m/s}$ is the number of monomers per segment, m is the molecular weight of a single monomer unit and $(\alpha_1 - \alpha_2)$ is the optical anisotropy of a segment. For aPS, n_o is quoted as 1.6[46] and $(\alpha_1 - \alpha_2)$ is quoted[45] as -145×10^{-25}. Δn_o depends on the concentration of polymer in solution, but not on the molecular weight of the polymer. For aPS, $m = 104$ and $N_{m/s} = 7.9$ in an ideal solvent[45].

The substitution of these values into equation (13) gives:

$$\Delta n_o(\text{aPS}) = -0.096c \quad (14)$$

Peterlin has pointed out that this expression neglects any contribution from the form anisotropy[47]. Form birefringence arises if the refractive index of the macromolecule differs from that of the solvent, creating a directional dependence of the velocity of light through the medium as a whole. Flow birefringence measurements are therefore composed of contributions from intrinsic and form birefringence.

Tsvetkov has calculated an expression for the additional segmental anisotropy due to the form effect, $(\alpha_1 - \alpha_2)_{fs}$[48]:

$$(\alpha_1 - \alpha_2)_{fs} = \left(\frac{n_o^2 - n_s^2}{4\pi n_s}\right)^2 (L_2 - L_1)\frac{N_{m/s} m}{\rho N_A} \quad (15)$$

where n_s is the refractive index of the solvent, $(L_2 - L_1)$ is a known function of the segmental axial ratio and ρ is the density of the polymer. For aPS in decalin[45], $n_s = 1.474$, $\rho = 1.05\,\text{g cm}^{-3}$ and $(L_2 - L_1) = 5$, and the birefringence of a fully stretched molecule becomes:

$$\Delta n_o(\text{aPS})_{dek} = -0.078c \quad (16)$$

The form anisotropy acts to increase the overall birefringence (i.e. make it more positive).

For a 0.02% ($c = 2 \times 10^{-4}$) solution, and using equation (16), the theoretical maximum should be -1.56×10^{-5}, which is smaller (less negative) than the experimentally obtained value. However, the form effect may not be the only complication. Frisman and Dadivanian have measured the segmental anisotropy, $(\alpha_1 - \alpha_2)$, of a series of macromolecules in different solvents by streaming birefringence[49]. Their results show a strong dependence of the measured segmental anisotropy arising from solvent anisotropy, rather than from changes in macromolecular conformation. They postulated that there was short-range ordering of the solvent molecules about the macromolecular chain, which affected the measured $(\alpha_1 - \alpha_2)$ values. Such short-range order becomes more pronounced in cases where polymer–solvent interactions are favourable. Decalin was found to provide the least positive value of $(\alpha_1 - \alpha_2)$ for polyethylene (PE) solutions.

Gent has calculated values of $(\alpha_1 - \alpha_2)$ from the stress-optical coefficient, C, for *cis*- and *trans*-polyisoprene samples, swollen to a high degree in a variety of non-polar solvents[50]. The results show a substantial variation in C [and hence $(\alpha_1 - \alpha_2)$] for the different swelling liquids. Some of the swelling agents gave an $(\alpha_1 - \alpha_2)$ value which was lower than for the unswollen material, whereas others generated an increase in the optical anisotropy. Gent concluded that the effect was due to the anisotropy of shape of the swelling liquids, and postulated a simple packing effect of the asymmetric solvent molecules in the vicinity of the polymer chain provides short-range orientational order. Gent also found the $(\alpha_1 - \alpha_2)$ value for decalin to be lower than the values for all the other liquids considered for *trans*-polyisoprene.

Clearly the prediction of birefringence values of fully stretched molecules in solution is a complex subject. The theoretical value of the birefringence of fully stretched aPS molecules in decalin, including the form effect, is seen to be less negative than the experimental values. A tentative prediction from the data given on short-range order suggests that the contribution to the optical anisotropy due to this effect for decalin, may be negative in sign, so that the theoretical maximum birefringence would more closely agree with the experimental maximum birefringence. Due to the fact that the Δn_{max} *versus* $\dot{\epsilon}$ curves in this work are found to plateau, and the Δn_{max} value at the plateau is of the same order as theoretical expectations (*Figure 7*), some degree of confidence can be asserted in the assumption that the molecules are being fully oriented.

In TCP, due to severe flow modification (*Figure 9*), the maximum experimental birefringence cannot be reliably related to the birefringence of fully stretched aPS molecules. However, the experimental data may be interpreted as showing a plateau at $\dot{\epsilon}_{nom} \approx 700\,\text{s}^{-1}$, for which $\Delta n_{max} = (3.7 \pm 0.1) \times 10^{-6}$. The theoretical calculation for the birefringence of fully extended aPS in TCP, for the given concentration, is 4.5×10^{-6}. This value takes into account the form effect but does not include an assessment of any possible optical anisotropy contribution from oriented solvent molecules.

For PEO, Dyakonova *et al.* have derived an expression for the maximum birefringence of fully extended molecules in water[51].

$$\Delta n_o = 4.12 \times 10^{-2}.c \quad (17)$$

where c is the polymer concentration in g cm^{-3}. The above expression takes into account the form birefringence, which was found to be ≈36% of the total Δn_o ($n_{PEO} = 1.46$ and $n_{water} = 1.338$). Using equation (17), the birefringence of fully stretched PEO molecules in aqueous solution, at a concentration $c = 2 \times 10^{-4}$, should be 0.824×10^{-5} (note that this value does not take into account any possible contribution to the optical segmental anisotropy from the bound water layer[52,53]). The measured value of Δn_{max} at $\dot{\epsilon}_{nom} = 59\,000\,\text{s}^{-1}$ is 0.96×10^{-5} (*Figure 11*).

Equilibrium conformation of extended macromolecules

Figure 12 is a plot of the maximum (plateau) experimental birefringence against molecular weight for four aPS samples in decalin, which reveals a striking, linear relationship. An explanation for this is that the equilibrium conformation of the molecule is not fully extended.

The application of Stokes law to an extended molecule (visualized as an extended string of beads) in a velocity gradient can be shown to produce a parabolic stress

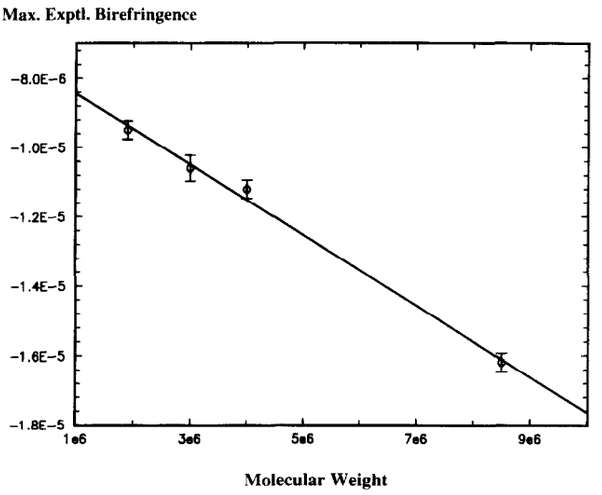

Figure 12 Maximum experimental (plateau) birefringence plotted against molecular weight, for 0.01% aPS/decalin solutions (metal jets apparatus)

distribution along the polymer chain, with the maximum stress at the centre of the chain. Moving outwards from the chain centre, the stress falls off until it reaches a level that cannot overcome the entropic restoring force of the chain, and therefore the chain segments beyond this limit form a more coil-like region. Thus, the equilibrium conformation of an 'extended' polymer molecule may resemble a fully stretched central region, with random coil-like structures at the chain ends. This picture has been previously presented by de Gennes[6].

In the flow field, the chain segments away from the chain centre are subject to a local extensional force arising from the relative solvent velocity. From the Stokes law analysis, $\nu_f \propto \dot{\epsilon}.M$, where ν_f is the relative solvent velocity, $\dot{\epsilon}$ is the strain rate and M is the molecular weight. For a given Deborah number, $\dot{\epsilon} \propto 1/M^{1.5}$, and it follows that $\nu_f \propto 1/M^{0.5}$. Assuming that the radius of the coiled end regions, r_{coil}, is inversely proportional to ν_f (although a higher exponent than 1 may be involved), it follows that $r_{coil} \propto M^{0.5}$. The proportion of the molecule that is coiled is therefore $\propto 1/M^{05}$. Thus, the higher the molecular weight, the lower the proportion of coiled chain segments and the higher the birefringence of the equilibrium extended conformation. This trend follows that of the relationship shown in *Figure 12*.

Extensional viscosity results

aPS in decalin; extensional viscometry. Pressure drop measurements were taken for aPS/decalin solutions in the vacuum driven apparatus. *Figure 13* shows the pressure drop across the jets, ΔP, as a function of strain rate, $\dot{\epsilon}$, for decalin (glass jets geometry). The quadratic fit to the experimental data is also indicated, along with the inertially corrected curve ($\Delta P - \Delta P_I$).

Figure 14 shows the ($\Delta P - \Delta P_I$) *versus* $\dot{\epsilon}$ trace for a 0.02% $M_p = 8 \times 10^6$ aPS/decalin solution, along with the inertially corrected trace for decalin. The deviation of the polymer solution curve from the expected behaviour of the Newtonian solvent is highly apparent. *Figure 15* presents the relative effective extensional viscosity (η'_e), which has been derived from *Figure 14*. The $(\eta'_e)_r$ curve increases to a plateau value of approximately 3.4 at

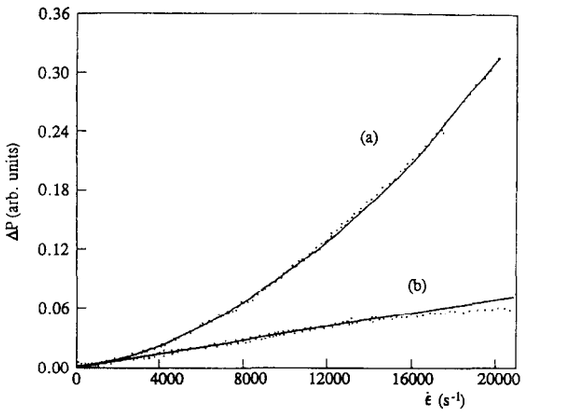

Figure 13 (a) Pressure drop (ΔP) *versus* strain rate ($\dot{\epsilon}$) for pure decalin in the glass jets apparatus. Data points: experimental data. Solid line: second order polynomial fit. (b) Data from (a) with the inertial component (ΔP_I) subtracted

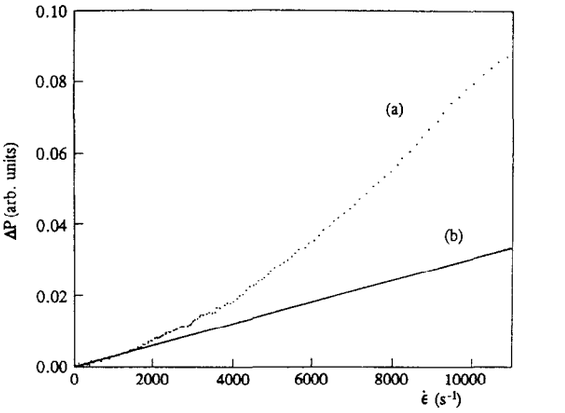

Figure 14 ($\Delta P - \Delta P_I$) *versus* strain rate ($\dot{\epsilon}$) for (a) 0.02% $M_p = 8 \times 10^6$ aPS/decalin solution and (b) decalin, in the glass jets apparatus

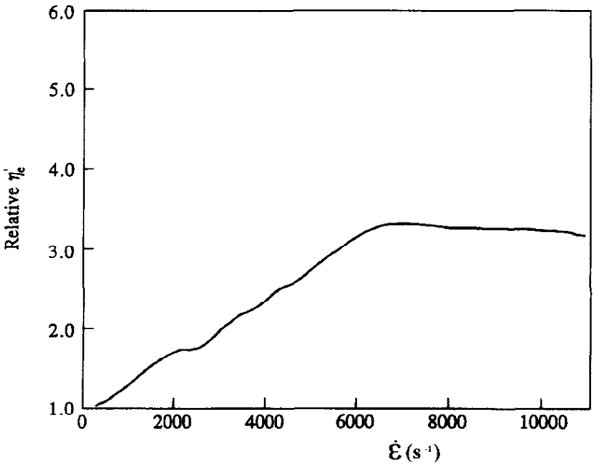

Figure 15 Relative extensional viscosity plot for 0.02%, $M_p = 8 \times 10^6$ aPS/decalin solution in the glass jets apparatus, derived from *Figure 14* (decalin viscosity = 1)

$\dot{\epsilon}_{nom} = 7000\,s^{-1}$. The retardation and birefringence profiles for this solution exhibit pronounced central dips above $\dot{\epsilon}_{nom} \approx 4500\,s^{-1}$, which have been attributed to screening effects caused by greatly enhanced local viscosity. Thus, the measured extensional viscosity cannot be considered to be a well-defined quantity.

The relative effective extensional viscosity, $(\eta'_e)_r$, can be converted to an effective intrinsic extensional viscosity, $[\eta'_e]$, using equation (11). The value obtained must then be corrected to take into account the effective area of molecular extension. An approximate correction may be obtained by scaling $[\eta'_e]$ as:

$$[\eta'_e]_{corr} = [\eta'_e] \times \frac{r_j^2}{r_s^2} \tag{18}$$

where r_j is the inner jet radius ($r_j = 0.175$ mm in the glass jets) and r_s is the radius of the region of significantly extended molecules. However, definiton of r_s is difficult since birefringence is not linearly related to molecular extension. A first approximation can be made by considering r_s to be the half width (at half maximum height) of the birefringence *versus r* profile.

For the aPS solution under consideration, complications arise due to flow modification above $\dot{\epsilon}_{nom} = 4500\,s^{-1}$, with the birefringence profiles exhibiting pronounced central dips and increasing broadening. As well as making the determination of r_s difficult, the presence of flow modification casts doubt on the validity of scaling the measured viscosity by the area of significant molecular extension. However, by selecting a strain rate at which flow modification is not apparent, some estimate of r_s can be made. For example, at $\dot{\epsilon}_{nom} = 3500\,s^{-1}$, $(\eta'_e)_r \approx 2.1$. The peak birefringence at this strain rate was ≈80% of the final value and, therefore, the solution concentration has been scaled accordingly in the evaluation of $[\eta'_e]$. The value of r_s is ≈0.015 mm, so that $[\eta'_e]$ should be corrected by a factor of 136. The division of $[\eta'_e]_{corr}$ by 3 times the intrinsic viscosity ($[\eta] = 218\,ml\,g^{-1}$, using the Mark–Houwink relationship $[\eta] = KM^a$, with parameters $K = 77 \times 10^{-3}\,ml\,g^{-1}$ and $a = 0.5$ for aPS in decalin at 18°C[46]) generates an estimate of the normalized extensional viscosity for aPS of approximately 1390. For this aPS sample, $N \approx 8000$, and the estimate for H is of the order of N.

Müller *et al.* obtained a normalized extensional viscosity, $H = 92$ for an aPS/decalin sample ($M_p = 4.4 \times 10^6$)[54]. The conclusion of this work was that values of H of the order of N were unlikely to arise from the coil–stretch transition alone, and intermolecular entanglements would be necessary to provide large values of H. However, the use of a sophisticated birefringence analysis to provide a correction for the region of significant molecular extension, has demonstrated that values of H which approach N may be obtained, but there is no firm evidence to suggest that higher powers of N may be generated. However, it is worth noting that a more realistic correction for the area of significant molecular stretching may be obtained if the measured birefringence profiles can be transformed into molecular strain profiles[34].

aPS in TCP; extensional viscometry. Pressure drop measurements for the aPS/TCP solution (0.005% $M_p = 8.5 \times 10^6$) were taken in the pressurized apparatus with the metal jets. The use of a high viscosity solvent, such as TCP, would be expected to eliminate (or certainly reduce) some of the problems associated with ΔP measurement in the opposed jets. The main advantages would be diminished inertial effects (the Reynolds number would be reduced for a given strain rate), and the strain rates required to stretch the molecules would be lowered (since $\dot{\epsilon}_c \propto 1/\eta_s$). High strain rates can be achieved with high viscosity solvents in the pressurized apparatus, because the available pressure drop allows the necessary flow rates to be obtained (the pressure drops are prohibitively large for the vacuum driven system to be used). The strain rate in the pressurized system can also be accurately controlled at low values.

The pressure drop across the jets, ΔP, as a function of strain rate, $\dot{\epsilon}$, for TCP was found to be linear, which implies that the flow is within the viscous limit, i.e. inertial effects are negligible.

An estimate was made of the extensional viscosity of TCP (neglecting any shear contribution to the pressure drop). A value of $\eta_e \approx 2.9$ Pa s was obtained, which is approximately 60 times the value of the shear viscosity. There still appears to be a large unexplained contribution to ΔP, and the implication of the result from the low Reynolds number TCP analysis is that this may be viscous in origin.

For the aPS/TCP solution, the flow field was significantly modified (*Figure 9*), which means that the measured extensional viscosity was not a well defined quantity. Using a similar analysis to the aPS/decalin solution, the $(\eta'_e)_r$ value of 1.7 at $\dot{\epsilon}_{nom} = 175\,s^{-1}$ was used in the subsequent analysis of the normalized extensional viscosity (the retardation profiles at this strain rate were single peaks). The peak birefringence at this strain rate was ≈80% of the maximum value, and therefore the solution concentration has been appropriately scaled in the evaluation of $[\eta'_e]$. For the metal jets, $r_j = 0.3$ mm. A first estimate for the value of r_s was taken as the half width, at half maximum height, of the birefringence *versus r* profile at $\dot{\epsilon}_{nom} = 175\,s^{-1}$, which gives $r_s \approx 0.029$ mm. Therefore, the correction factor for $[\eta'_e]$ is 107. The intrinsic viscosity of aPS was estimated from published data[40,55,56], and a value of $[\eta] = 600\,ml\,g^{-1}$ was assumed. The division of $[\eta'_e]_{corr}$ by 3 times the intrinsic viscosity provided an estimate of the normalized extensional viscosity (H) for aPS of approximately 1040, which again is of the order of N.

CONCLUSIONS

The improvements in apparatus design realize better flow control and much improved spatial resolution of flow induced retardation around the stagnation point. This coupled with an iterative transform process permits the recovery of absolute birefringence as a function of radial position. At all but the lowest concentrations, pronounced screening effects are observed, where the local increase in extensional viscosity produces significant flow modification with a reduced strain rate around the stagnation point. The screening is particularly strong for high molecular weights and good solvents.

At concentrations low enough to be considered truly dilute ($\approx c^*/100$) a well behaved, localized birefringence is observed. The onset of stretching shows a critical strain rate and a sigmoidal profile with increasing strain rate. The width of the transition is consistent with the known polydispersity of the polymers used. The final plateau level of birefringence is of the same order as the theoretical values expected for fully oriented polymers, including form birefringence but subject to the uncertainties of solvent effects.

After allowance for the area of strongly birefringent molecules, the effective extensional viscosity shows an

enormous increase ($\approx$ 1000-fold) during the stretching transition. This is of the order of N, the number of equivalent flexible links in the chain.

The observations point to a critical coil–stretch transition with a high degree of stretching of the molecules around the stagnation point. In a following paper[34], we present an analysis of the flow field coupled with a derivation of molecular strain. This allows a comparison of molecular and fluid strain, and follows the evolution of molecular extension in a quasi-steady state flow field.

ACKNOWLEDGEMENTS

We gratefully acknowledge the financial support of BP Venture Research and EPSRC. We are grateful for many useful discussions with Prof. A. J. Müller.

REFERENCES

1. Fabula, A. G., Hoyt, J. W. and Crawford, H. R., *Bulletin, APS*, 1963, 8.
2. Dauben, D. L. and Menzie, D. E., *J. Petroleum Tech.*, 1967, **19**, 1065.
3. James, H. M. and Guth, E., *J. Chem. Phys.*, 1943, **11**, 455
4. Flory, P. J., *J. Chem. Phys.*, 1942, **10**, 51.
5. Peterlin, A., *Makr. Chem.*, 1961, **44–46**, 338.
6. De Gennes, P. G., *J. Chem. Phys.*, 1974, **60**, 5030.
7. Hinch, E. J., *Polymères et Lubrification, Colloques Internationaux du CNRS* 233, 1974, 241.
8. Brestkin, Yu. V., *Acta Polym.*, 1987, **38**, 470.
9. Magda, J. J., Larson, R. G. and Mackay, M. E., *J. Chem. Phys.*, 1988, **89**, 2504.
10. Wiest, J. M., Wedgewood, L. E. and Bird, R. B., *J. Chem. Phys.*, 1989, **90**, 587.
11. Fan, X.-J., Bird, R. B. and Renardy, M., *J. Non-Newtonian Fluid Mech.*, 1985, **18**, 255.
12. Liu, T. W., *J. Chem. Phys.*, 1989, **90**, 5826.
13. Darinskii, A. A., Lyulin, A. V. and Saphiannikova, M. G., *Int. J. Polymeric Mater.*, 1993, **22**, 15.
14. Rallison, J. M. and Hinch, E. J., *J. Non-Newtonian Fluid Mech.*, 1988, **29**, 37.
15. Hinch, E. J., *J. Non-Newtonian Fluid Mech.*, 1994, **54**, 209.
16. Pope, D. P. and Keller, A., *Colloid Polym. Sci.*, 1978, **255**, 633.
17. Keller, A. and Odell, J. A., *Colloid Polym. Sci.*, 1985, **263**, 181.
18. Taylor, G. I., *Proc. Roy. Soc. Lond.*, 1934, **A146**, 501.
19. Odell, J. A., Keller, A. and Müller, A. J., *Advances in Chemistry*, 1989, **223**, 193.
20. Cathey, C. A. and Fuller, G. G., *J. Non-Newtonian Fluid Mech.*, 1990, **34**, 63.
21. Fuller, G. G. and Leal, L. G., *J. Polym. Sci. Polym. Phys. Ed.*, 1981, **19**, 557.
22. Dunlap, P. N. and Leal, L. G., *J. Non-Newtonian Fluid Mech.*, 1975, **23**, 5.
23. Brestkin, Yu. V., Saddikov, I. S., Agranova, S. A., Baranov, V. G. and Frenkel, S., *Polym. Bull.*, 1986, **15**, 147.
24. Carrington, S. P., Ph.D. Thesis, University of Bristol, 1995.
25. Odell, J. A. and Keller, A., *J. Polym. Sci., Polym. Phys. Ed.*, 1986, **24**, 1889.
26. Odell, J. A., Keller, A. and Rabin, Y., *J. Chem. Phys.*, 1988, **88**, 4022.
27. Odell, J. A., Müller, A. J., Narth, K. A. and Keller, A., *Macromolecules*, 1990, **23**, 3092.
28. Narh, K. A., Odell, J. A., Müller, A. J. and Keller, A., *Polym. Commun.*, 1990, **31**, 2.
29. Odell, J. A. and Taylor, M. A., *Biopolymers*, 1994, **34**, 1483.
30. Larson, R. G., Perkins, T. T., Smith, D. E. and Chu, S., *Phys. Rev. Lett.* (submitted).
31. Nguyen, T. Q., Yu, G. and Kausch, H. H., *Macromolecules*, 1995, **28**, 4851.
32. Menasveta, M. J. and Hoagland, D. A., *Macromolecules*, 1991, **24**, 3427.
33. Cooper, S., Ph.D. Thesis, University of Leeds, 1995.
34. Carrington, S. P., Tatham, J. P., Sáez, A. E. and Odell, J. A., *Polymer*, in press.
35. Riddiford, C. L. and Jerrard, H. G., *J. Phys. D.: Appl. Phys.*, 1970, **3**, 1314.
36. Carrington, S. P. and Odell, J. A., *J. Non-Newtonian Fluid Mech.*, 1996, **67**, 269.
37. Tatham, J. P., Ph.D. Thesis, University of Bristol, 1993.
38. Müller, A. J., Ph.D. Thesis, University of Bristol, 1989.
39. Fuller, G. G., Cathey, C. A., Hubbard, B. and Zebrowski, B. E., *J. Rheol. (USA)*, 1987, **31**, 235.
40. Riande, E., Markovitz, H., Plazek, D. J. and Raghupathi, N., *J. Polym. Sci.: Symp.*, 1975, **50**, 405.
41. Bailey, F. E. (Jr.) and Koleske, J. V., *Poly(ethylene oxide)*. Academic Press, New York, 1976.
42. Ng, R. C. Y. and Leal, L. G., *J. Rheol.*, 1993, **37**, 443.
43. Harlen, O. G., Hinch, E. J. and Rallison, J. M., *J. Non-Newtonian Fluid Mech.*, 1992, **44**, 229.
44. Treloar, L. K. G., *The Physics of Rubber Elasticity*, 3rd edn Clarendon Press, Oxford, 1975.
45. Tsvetkov, V. N., Eskin, V. E. and Frenkel, S. Ya., *Structure of Macromolecules in Solution*, Vol. 3, (Transl. and Ed. Crane-Robinson). National Lending Library for Science and Technology, Boston Spa, 1971.
46. Brandrup, J. and Immergut, E. H., *Polymer Handbook*, 3rd edn. Wiley Interscience, New York, 1989.
47. Peterlin, A., *Polymer*, 1961, **2**, 257.
48. Tsvetskov, V. N., *Vysokomol. Soyed*, 1963, **5**, 740.
49. Frisman, E. V. and Dadivanian, A. K., *J. Polym. Sci. Part C*, 1967, **16**, 1001.
50. Gent, A. N., *Macromolecules*, 1969, **2**, 262.
51. Dyakanova, N. E., Brestkin, Yu. V., Agranova, S. A., Pogrebnyak, V. G. and Tverdokhleb, S. V., *J. Polym. Sci. (USSR)*, 1989, **31(B)**, 844.
52. Liu, K. J. and Parsons, J. L., *Macromolecules*, 1969, **2** 529.
53. Maxfield, J. and Sheperd, I. W., *Polymer*, 1975, **16**, 505.
54. Müller, A. J., Odell, J. A. and Keller, A., *J. Non-Newtonian Fluid Mech.*, 1988, **30**, 99.
55. Lodge, T. P., Hermann, K. C. and Landry, M. R., *Macromolecules*, 1986, **19**, 1996.
56. van Brandwijk, R. A. M., Hesse, M. G. L., Jalink, H. L. and Peeters, F. A. H., *Bull. Soc. Chim. Belg.*, 1981, **90**, 105.